from activated sludge. ND-11 completely degraded the polyamide film in 2 weeks. With the ND-11 enzyme, γ-aminobutyric acid can be recovered by hydrolysis, and PRN also can be recovered by thermal decomposition of the polymer (chemically recyclable). Biodegradations of PA4 in soil and compost were also reported [15,16]. PA4 has a higher melting temperature and excellent tensile strengths than those of PA6 because of its short repeating unit. However, it is rather brittle and an elongation at break is 10–30% [17]. Furthermore, thermal decomposition temperature is close to *T*m. To solve these issues, copolymer is one of the promising ideas. In this paper, we report the synthesis and biodegradation of the copolyesteramides which are biodegraded with any composition ratio.

2. Experimental

2.1. Reagents

PRN (2-pyrrolidone, Kishida) and CL (ε-caprolactone, Wako) were used after distillation under vacuum. *n*-Butyllithium hexane solution (*n*BuLi, 1.6 M, Wako) was used as an initiator without purification. The enzymes for the biodegradation tests were mainly a lipase from *Rhizopus delemar* (L-RA) (600–700 U/ml, Seikagaku Industries) and a proteinase K (20 U/mg, Wako).

2.2. Measurements

^{1}H NMR (500 MHz) and ^{13}C NMR (125 MHz) spectra were recorded on a Jeol JNM ECA-500 spectrometer. Polymer compositions were determined according to the calculations of the intensity ratio of the assigned peaks. Thermal analyses were performed on a DSC3100S differential scanning calorimeter (Bruker AXS, Japan). Samples of 2–8 mg (weighed into aluminum pans) were measured at a heating rate of 10 °C/min. Molecular weight distributions were determined by a Tosoh gel permeation chromatography system (HLC-8020) using polystyrene standards and chloroform as elution solvent. The columns were TSKgel G5000H$_{XL}$, G4000H$_{XL}$ and G3000H$_{XL}$ with a limited exclusion molecular weight of 4×10^6. When polymers did not dissolve in chloroform, hexafluoroisopropanol (Central Glass Co. Ltd.) was used as eluent with PMMA standards.

2.3. Polymerizations

The copolymerization of PRN with CL was carried out in bulk. Monomers were placed in a two-necked flask equipped with a condenser, a desiccant tube and a magnetic stirrer. *n*BuLi (0.2–1.6 mol% versus total monomers) was carefully added at 0 °C with vigorous stirring. The flask was heated up to room temperature or 50 °C for 3 days. Subsequently, they were allowed to cool down and the contents were dissolved in trifluoroethanol. The synthesized polymers were precipitated with methanol or acetone. Crude polymers were separated by filtration and finally dried under reduced pressure. A series of copoly(PRN/CL)s whose polymer composition was polyCL to polyPRN were synthesized.

2.4. Biodegradation test

Biodegradability was evaluated both by enzymatic hydrolyses and biological degradation tests. In the case of enzymatic hydrolysis, 25 mg of polymer samples and 2 ml of phosphate buffer (KH_2PO_4/Na_2HPO_4, pH 7.0, 0.1 M) were added into each of the three tubes. Then, 200 units of the lipase from *R. delemar* was added to the tubes with the exception of one for a control test. The hydrolysis was carried out at 37 °C for 24 h. After filtration (0.2 μm membrane filter), the total organic carbon concentration (TOC) was measured in duplicate. The averages of TOC data were corrected appropriately after subtraction of the blank levels [18]. Proteinase K was also used for hydrolysis test.

Another biodegradation of polymers was evaluated by a standard activated sludge and PA4 degrading bacterium ND-11. Evaluation was carried out through the determination of the amount of oxygen consumption using a BOD tester, 200F (Taitec). Typically, 100 mg of copolymers was added into BOD testing bottle, followed by 180 ml phosphate buffer, which was prepared according to ISO 14851, and 20 ml activated sludge (MLSS 20 mg/20 ml). The biodegradation test was carried out at 27 °C with stirring. The observed O_2 consumption volume was corrected by subtraction to that of the blank. Biodegradation (%) of polymers was calculated as a division of observed O_2 consumption volume by the theoretical one.

3. Results and discussion

3.1. Polymerization of copolyesteramides

The general scheme for the conversion of the involved monomers to polymer is as shown in Scheme 1. In 1968, Komoto et al. reported the copolymerization of copolyesteramides in the presence of alkali metal at 40 °C [19]. They used amide salts produced from alkali metal with lactams, and they showed high reactivity to ring-opening polymerization of lactams. Several kinds of amide salts were reported for production of copolyesteramides, such as ε-caprolactam/CLN [20,21]. On the contrary, basicity of *n*BuLi is not high compared with alkali metal. However, it is reactive with lactones. Therefore, to obtain high molecular weight, we consider usage of *n*BuLi with long reaction time at mild temperature. The yields of bulk polymer syntheses after precipitation and the NMR determination of the PRN/CL (molar ratio) in the polymer are given in Table 1. In most cases, polymerization was carried out at room temperature because the high temperature (>50 °C) was undesirable for polymerization of PRN and a low molecular weight copolymer was obtained (run 10) [17]. When 0.24 mol% of *n*BuLi was used, polymerization of PRN did not proceed completely and PRN content in the copolymer and molecular weight were low (run 3). As for purification, precipitants were not obtained with methanol in the feed range of 80/20 to 35/65, therefore, acetone was used for reprecipitation. When acetone was used, the yields increased and the copolymer composition was in satisfactory agreement with the comonomer feed ratio. However, the molecular weights decreased (runs 1, 2, 11 and 12). To measure *Mn* and *Mw*, chloroform was used for CL-rich polymers as an eluent, and hexafluoroisopropanol (HFIP) was used for PRN-rich polymers because

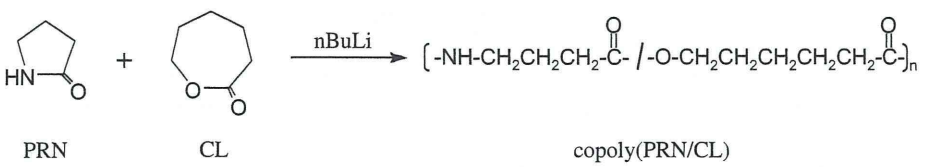

Scheme 1. Synthesis of copoly(PRN/CL).

Please cite this article in press as: Nakayama A, et al., Synthesis and biodegradation of poly(2-pyrrolidone-*co*-ε-caprolactone)s, Polymer Degradation and Stability (2013), http://dx.doi.org/10.1016/j.polymdegradstab.2013.04.011

Table 1
Copolymerization of 2-pyrollidone (PRN) with ε-caprolactone (CL).

Run No.	PRN/CL mol ratio	BuLi (mol%)	Temp. (°C)	Time (d)	Yield (%)	Polymer comp.[a] PRN/CL	Mn^b ($\times 10^3$)	Mw^b ($\times 10^3$)	Mw/Mn^b	Solv. for reprecipitation
1	100/0	0.8	rt	3	29	100/0	6.3	18.3	2.90	Acetone
2	100/0	0.8	rt	3	25	100/0	9.9	23.7	2.40	Methanol
3	90/10	0.24	rt	3	22	72/28	9.0	22.9	2.55	Methanol
4	90/10	0.8	rt	3	82	92/8	13.1	38.5	2.94	Methanol
5	90/10	1.6	rt	3	82	91/9	12.2	34.5	2.84	Methanol
6	80/20	0.8	rt	3	82	77/23	13.2	40.3	3.04	Acetone
7	70/30	0.8	rt	3	86	65/35	13.1	38.5	2.95	Acetone
8	60/40	0.8	rt	3	61	54/46	9.1	25.6	2.82	Acetone
9	50/50	0.8	rt	3	65	44/56	12.9	35.5	2.74	Acetone
10	50/50	0.8	50	3	25	49/51	8.7	25.8	2.98	Acetone
11	35/65	0.8	rt	3	62	35/65	7.6	24.7	3.26	Acetone
							11.4	*25.3*	*2.23*	
12	35/65	0.8	rt	3	37	18/82	15.0	34.9	3.33	Methanol
							27.9	*37.5*	*1.34*	
13	25/75	0.8	rt	3	44	14/86	9.7	26.5	2.73	Methanol
							20.7	*33.9*	*1.63*	
14	10/90	0.8	rt	3	70	2/98	4.1	10.5	2.59	Methanol
							13.4	*20.3*	*1.52*	
15	0/100	0.8	rt	3	75	0/100	*13.1*	*70.9*	*5.42*	Methanol

[a] Calculated by ^{1}H NMR measurement.
[b] Hexafluoroisopropanol (HFIP) was used as an eluent. In case of italic values, chloroform was used instead of HFIP.

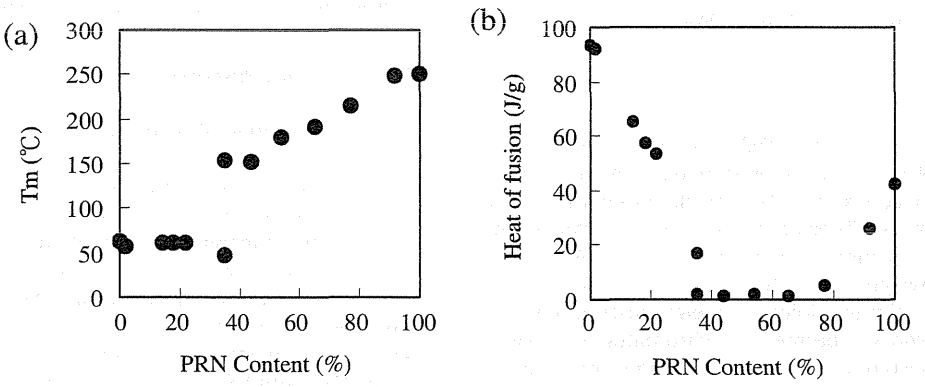

Fig. 1. Results of DSC measurement of the copoly(PRN/CL)s: (a) melting temperature (*Tm*); (b) heat of fusion.

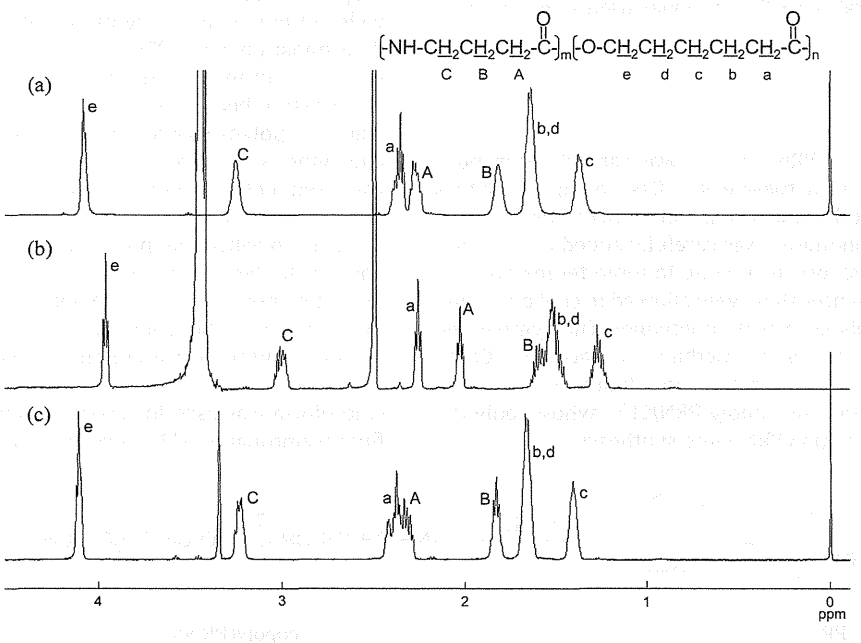

Fig. 2. Comparison of ^{1}H NMR spectra of the copolymer (feed ratio, PRN/CL = 50/50, run 9 in Table 1) measured in three different deuterium solvents: (a) $CDCl_3$/DCOOD (9/1); (b) d_6-DMSO; (c) CD_3OD/LiCl.

Please cite this article in press as: Nakayama A, et al., Synthesis and biodegradation of poly(2-pyrrolidone-*co*-ε-caprolactone)s, Polymer Degradation and Stability (2013), http://dx.doi.org/10.1016/j.polymdegradstab.2013.04.011

they were not soluble to chloroform. Molecular weights with chloroform were larger than those with HFIP (runs 11–14). The DSC results show that PRN-rich copolymers have a relatively high *T*m (higher than 200 °C), whereas CL-rich copolymers have lower *T*m (around 60 °C) (Fig. 1). The melting temperatures of copolymers were similar values to those reported by Komoto. The heats of fusion of copoly(PRN/CL)s were very small at the copolymers region.

3.2. Structure of copolymers

The ^{1}H NMR spectra of the copoly(PRN/CL) (feed PRN/CL = 50/50) using several d-solvent and the assignment are shown in Fig. 2. In all cases, calculated polymer compositions show almost same results, that is, (a) PRN/CL = 44/56, (b) 45/55 and (c) 45/55, respectively. However, chemical shifts of the observed signals were dependent on the solvent. α-Methylene protons in PRN and CL units of the copolymers in DMSO were observed at 2.03 and 2.26 ppm and their coupling seems simple dd. On the contrary, with methanol/LiCl, the coupling patterns at α-methylene protons (2.45–2.28 ppm) were complicated. However, it is failed to separate the peaks of diad hetero sequences (–CL–PRN– and –PRN–CL–) from diad homo sequences (–CL–CL– and –PRN–PRN–). Therefore, ^{13}C NMR spectra were examined (Fig. 3). Carbon peaks in PRN and CL units derived from diad homo sequences were confirmed with those of each homopolymer. Every carbon peak composes a pair, that is, diad homo and diad hetero carbons. As increase of PRN content, intensities of homo peaks in CL unit decreased and the other hetero peaks increased. On the contrary, homo peak intensities in PRN unit increase as increase of PRN content. Some hetero signals were split, and they are explained as triad hetero sequences. Each homo/hetero intensity ratio shows a similar value in the same copolymer. PRN and CL block lengths can be calculated as the division of the total of homo and hetero peak intensities by a hetero intensity. In case of PRN/CL = 44/56 (run 9 in Table 1), the block length of PRN unit is calculated as 2.31 and that of CL unit is 2.46. Therefore, they were not perfectly random, but random-like copolymers, which composed of short homo sequences of PRN and CL. The block lengths of the other two copolymers are, run 14; PRN = 1.0, CL = 40, run 6; PRN = 5.34, CL = 1.56. The ratio of block length (PRN/CL) shows good agreement with polymer composition ratio, PRN/CL.

3.3. Biological biodegradation of the copolymers

The biodegradability of the obtained copolymers was evaluated using the PA4-biodegrading microorganism, ND-11, which was isolated from activated sludge and identified as a pseudomonas sp [12]. The biodegradation mechanism of PA4 was clarified as a two-

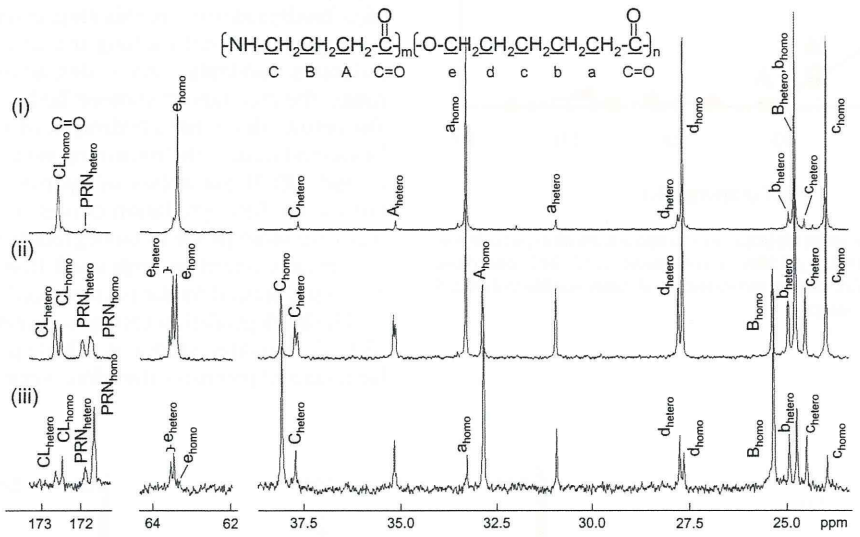

Fig. 3. ^{13}C NMR spectra of copoly(PRN/CL)s measured in d_6-DMSO: (i) PRN/CL = 2/98 (run 14 in Table 1); (ii) PRN/CL = 44/56 (run 9 in Table 1); (iii) PRN/CL = 77/23 (run 6 in Table 1).

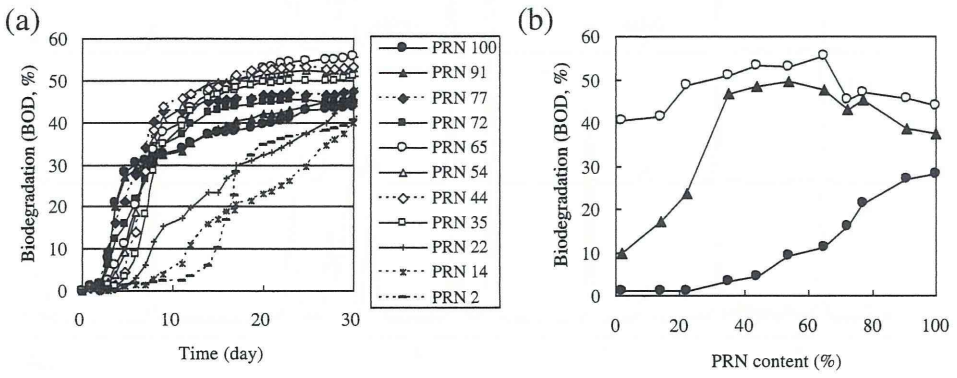

Fig. 4. Biodegradation of a series of copoly(PRN/CL)s by PA4-biodegrading microorganism, ND-11 at 23 °C. Biodegradation was evaluated by biological oxygen demand. (a) Biodegradation profile; (b) Relationships between biodegradation and PRN content in copolymers. (●) 5 days; (▲) 15 days; (○) 30 days.

Please cite this article in press as: Nakayama A, et al., Synthesis and biodegradation of poly(2-pyrrolidone-*co*-ε-caprolactone)s, Polymer Degradation and Stability (2013), http://dx.doi.org/10.1016/j.polymdegradstab.2013.04.011

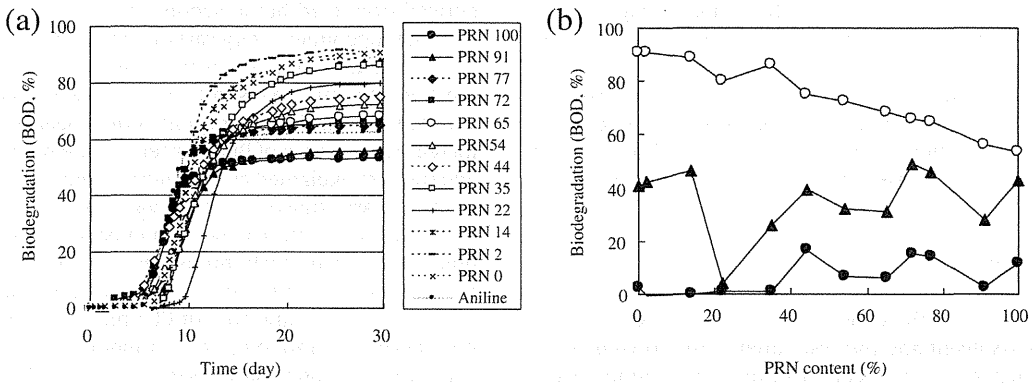

Fig. 5. Biodegradation of a series of copoly(PRN/CL)s by activated sludge at 23 °C in inorganic medium stated in ISO 14851. Biodegradation was evaluated by biological oxygen demand. (a) Biodegradation profile; (b) Relationships between biodegradation and PRN content in copolymers. (●) 7 days; (▲) 10 days; (○) 30 days.

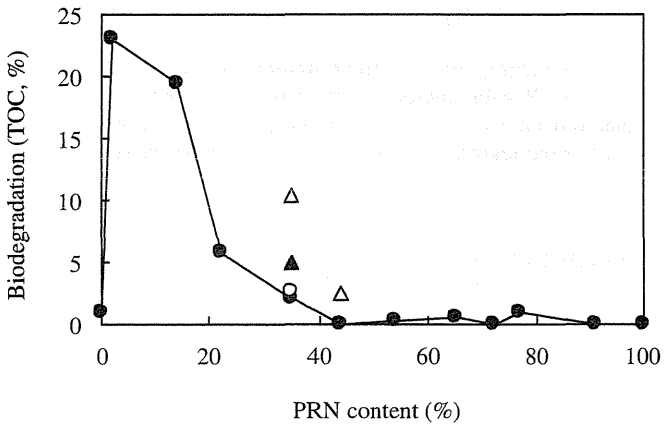

Fig. 6. Enzymatic hydrolysis of copoly(PRN/CL)s using a lipase from *Rhizopus delemar*: (●) 200 U; (○) 500 U; (▲) 1000 U; (△) 2000 U. Conditions: 37 °C; 24 h, phosphate buffer (pH 7). Hydrolysis was calculated by measurement of water-soluble hydrolyzed products concentration by TOC analyzer.

step degradation. At first, PA4 was hydrolyzed into γ-aminobutyric acid (GABA) by way of oligomers, and then GABA was metabolized to inorganic compounds.

The biodegradation results of the copolymers were shown in Fig. 4. The polymers were gradually biodegraded. At the beginning of test, PA4 and amide-rich copolymers were rapidly degraded whereas ester-rich copolymers were hardly biodegraded. And then, copolymers with the composition range 40–60% of PRN showed high biodegradation. In this step, ester-rich polymers did not start to degrade yet. With a long inductive period, PCL and ester-rich polymers suddenly started degradation, and in all composition range, the copolymers showed high biodegradation after 1 month. The results show that a hydrolysis of amide bond was predominant biodegradation at the beginning step, and then with long inductive period, ND-11 got ability of hydrolysis of ester bond during test. Finally, the biodegradation curves reached to flat, ester-rich polymers are more prone to biodegradation than amide-rich polymers. The results might be explained that nitrogen-rich polymers are easily introduced to the bacterial cell.

The biodegradation test by activated sludge was also carried out (Fig. 5). Activated sludge is a biological floc composed of aerobic bacteria and protozoa, therefore, several bacteria or protozoa could

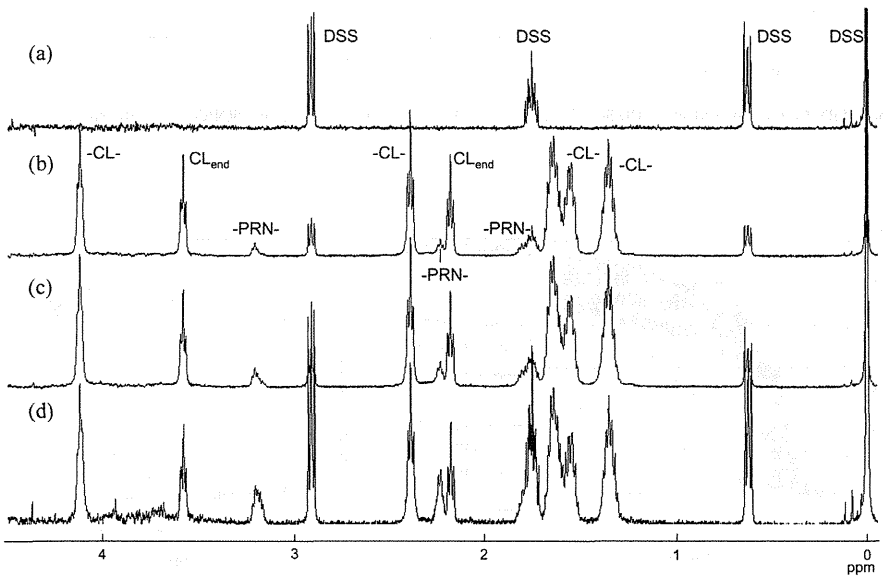

Fig. 7. ^{1}H NMR spectra of the water-soluble lipase-hydrolyzed products of the copolymers in D_2O using DSS as an internal standard. (a) Control of copoly(PRN/CL), (22/78); (b) copoly(PRN/CL), (2/98, run 14 in Table 1); (c) copoly(PRN/CL), (14/86, run 13 in Table 1); (d) copoly(PRN/CL), (22/78).

Please cite this article in press as: Nakayama A, et al., Synthesis and biodegradation of poly(2-pyrrolidone-*co*-ε-caprolactone)s, Polymer Degradation and Stability (2013), http://dx.doi.org/10.1016/j.polymdegradstab.2013.04.011

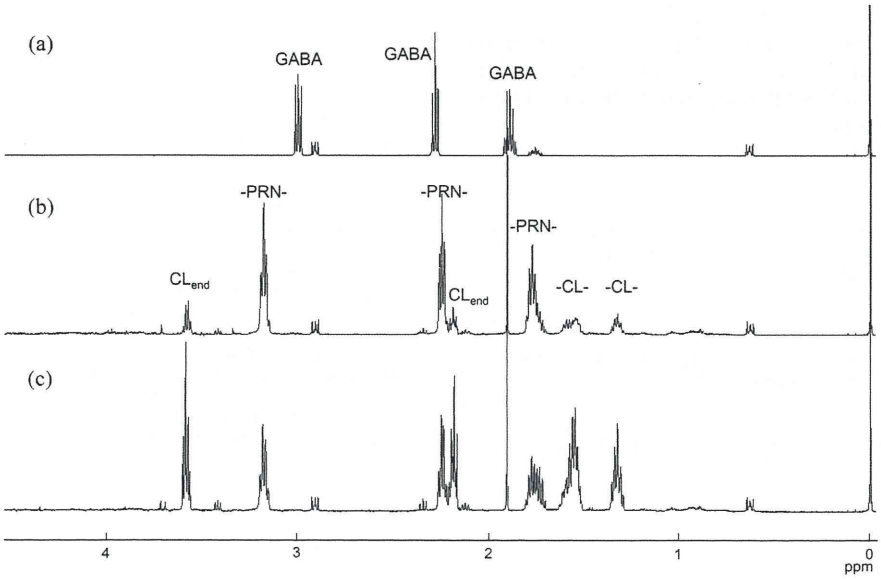

Fig. 8. ^{1}H NMR spectra of the water-soluble enzymatic hydrolyzed products by proteinase K of the copolymers in D_2O using DSS as an internal standard. (a) γ-aminobutylic acid; (b) copoly(PRN/CL), (91/9, run 5 in Table 1); (c) copoly(PRN/CL), (44/56, run 9 in Table 1).

biodegrade ester and amide compounds. Most of the polymers were started to be degraded in a week in contrast to the case of ND-11 (Fig. 5(a)). It means hydrolyzability of ester bond is as high as that of amide bond in PA4. The biodegradation curves reached to flat, 4 weeks later. Biodegradation tendency of the copolymers at 4 weeks were similar to that of ND-11 biodegradation. In this case, the results also might be explained that nitrogen-rich polymers are easily introduced to the bacterial cell.

3.4. Enzymatic hydrolysis

To evaluate hydrolyzability, enzymatic hydrolysis tests are performed. Fig. 6 shows the results of the copolyesteramides of various compositions using lipase from *R. delemar*. The measurement of hydrolyzability was based on the amount of water-soluble parts produced by hydrolysis and determined by TOC (total organic carbon concentration) measurement. The lipase-hydrolyzability was quite pronounced at the CL-rich region as compared with the PRN-rich region. The copolymer (PRN/CL = 2/98) showed the maximum hydrolyzability in the series. PCL was hydrolyzed much slowly compared with the copolymers. These results show that ester bonds are hydrolyzed by lipase. However, although copolymers with more than 40% PRN have still ester bonds in their backbone, they were hardly hydrolyzed. Water-soluble hydrolyzed products were analyzed by ^{1}H NMR. The filtrates tested were dried and were measured as a D_2O solution with DSS as an internal standard (Fig. 7). NMR spectrum of control of copoly(PRN/CL), (22/78) showed only signals of DSS and showed no characteristic signals. With the enzyme, methylene protons in CL unit derived from hydrolysis of ester bond were observed at 3.58 and 2.18 ppm in addition to the methylenes (4.12 and 2.39 ppm) in CL unit which were assigned as $-COO-CH_2-$ and $-OCO-CH_2-$. The ratios of PRN/CL of hydrolyzed products were 5/95 (b), 11/89 (c), and 23/77 (d), and they were in good agreement with those of original copolymers. The results strongly support the original copolymers were random. The hydrolyzed products are found to be dimer to tetramer of CL and PRN from analysis of intensity of end groups.

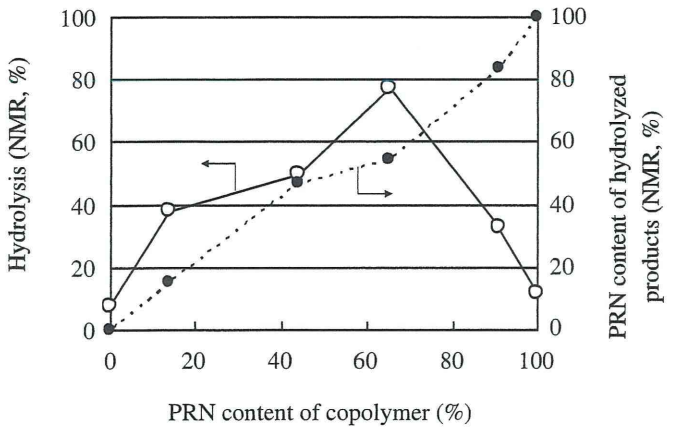

Fig. 9. Enzymatic hydrolysis of copoly(PRN/CL)s using 100 U of proteinase K. Conditions: 37 °C; 90 h, sample 20 mg, deuterium phosphate buffer (pH 7) 2 ml. Hydrolysis was calculated by ^{1}H NMR analysis of water-soluble hydrolyzed products.

Proteinase K was also used for hydrolysis test. Biodegradation was calculated by intensities of ^{1}H NMR peaks of water-soluble hydrolyzed products (Fig. 8). Fig. 9 shows the dependence of hydrolyzability on the polymer composition. The higher hydrolysis was recorded for the amorphous copolymers whose PRN content was in the range of 40–70 mol%. The optimum copolymer composition ratio for achieving maximum hydrolysis is PRN/CL = 56/44. Even a copolymer with 91% of PRN was also hydrolyzed, in contrast to lipase-hydrolysis. As for ^{1}H NMR spectra of the proteinase K-hydrolyzed products, the methylene peaks ($-O-CH_2-$) at 3.59 ppm were observed, not at 4.12 ppm. In addition, the peaks at 3.18, 2.24, and 1.76 ppm were assigned as methylene protons in PRN unit of the polymers because they were not equaled to those of γ-aminobutyric acid. These results suggest proteinase K predominantly effects on ester bonds compared to amide bond. The ester hydrolysis was not inhibited from amide bonds.

4. Conclusions

Novel biodegradable copolyesteramides were synthesized by ring-opening polymerization of PRN with CL. The synthesized polymers were random copolymers. The biodegradability was evaluated by enzymatic hydrolysis and biological degradation test by a PA4 degrading microorganism and activated sludge. As for

Please cite this article in press as: Nakayama A, et al., Synthesis and biodegradation of poly(2-pyrrolidone-*co*-ε-caprolactone)s, Polymer Degradation and Stability (2013), http://dx.doi.org/10.1016/j.polymdegradstab.2013.04.011

enzymatic hydrolysis, there is a suitable polymer composition for maximum degradation, but in case of biological degradation, with all composition range, copolymers were biodegraded well. These copolymers are expected to be eventually used as environmentally-friendly substitute materials.

References

[1] Beauprez JJ, Mey MD, Soetaert WK. Process Biochem 2010;45:1103–14.
[2] Kaur G, Srivastava AK, Chand S. Biochem Eng J 2012;64:106–18.
[3] Kricheldorf HR, Bornhorst K, Schellenberg J, Schwarz G. J Macromol Sci Part A 2007;44:119–24.
[4] Doi Y, Fukuda K. Biodegradable plastics and polymers. Stud Polym Sci 1994;12. [Elsevier].
[5] Matsumura S, Steinbuchel A. Miscellaneous biopolymers and biodegradation of polymers. Biopolymers 2001;9. [Wiley-VCH].
[6] Nakayama A, Ukita M, Iyoda J, Kawasaki N, Yamamoto N. Polym Deg Stab 2012;97:14–20.
[7] Petchsuk A, Nakayama A, Aiba S. Polym Deg Stab 2009;94:1700–6.
[8] Yamamoto N, Nakayama A, Oshima M, Kawasaki N, Aiba S. Reactive Funct Polym 2007;67:1338–45.
[9] Ando H, Oshima M, Nakayama Y, Nakayama A. Polym Deg Stab 2013;98:958–62.
[10] Belloncle B, Bunel C, Bouaouiche LM, Lesouhaitier O, Burel F. J Polym Environ 2012;20:726–31.
[11] Zheng L, Wang Z, Li C, Xiao Y, Zhang D, Guan G, et al. Polymer 2013;54:631–8.
[12] Yamano N, Kawasaki N, Takeda S, Nakayama A. J Polym Environ 2013;21:528–33.
[13] Yamano N, Nakayama A, Kawasaki N, Yamamoto N, Aiba S. J Polym Environ 2008;16:141–6.
[14] Kawasaki N, Yamano N, Takeda S, Ando H, Nakayama A. J Appl Polym Sci 2012;126:E425–32.
[15] Hashimoto K, Hamano T, Okada M. J Appl Polym Sci 1994;54:1579–83.
[16] Tachibana K, Hashimoto K, Yoshikawa M, Okawa H. Polym Deg Stab 2010;95:912–7.
[17] Kawasaki N, Nakayama A, Yamano N, Takeda S, Kawata Y, Yamamoto N, et al. Polymer 2005;46:9987–93.
[18] Tokiwa Y, Suzuki T, Ando T. J Appl Polym Sci 1979;24:1701–11.
[19] Komoto H. Makromol Chem 1968;115:33–42.
[20] Chromcova D, Baslerova L, Roda J, Brozek J. Eur Polym J 2008;44:1733–42.
[21] Toncheva N, Mateva R. Polym Bull 2008;60:27–36.

Please cite this article in press as: Nakayama A, et al., Synthesis and biodegradation of poly(2-pyrrolidone-co-ε-caprolactone)s, Polymer Degradation and Stability (2013), http://dx.doi.org/10.1016/j.polymdegradstab.2013.04.011

Stress Distribution in a Bilayer Elastic Model of a Coronary Artery

Keiichi Takamizawa[1]
e-mail: ktaka@ri.ncvc.go.jp

Yasuhide Nakayama

Department of Biomedical Engineering,
National Cerebral and Cardiovascular
Center Research Institute,
5-7-1 Fujishirodai, Suita,
Osaka 565-8565, Japan

In earlier studies on stress distribution in arteries, a monolayer wall model was often used. An arterial wall consists of three layers, the intima, the media, and the adventitia. The intima is mechanically negligible as a stress supporting layer against the blood pressure in young healthy vessels, although it is important as an interface between blood and arterial wall. The media and adventitia layers are considered to support blood pressure. Recently, residual strain and a constitutive law for porcine coronary arteries have been investigated in separated media and adventitia. Using the data obtained through these investigations, a stress analysis considering residual stress (strain) in each layer was performed in this study, and residual strain and stress were computed for a bilayer model. The circumferential residual stress was compressive in the inner region, tensile in the outer region, and had discontinuity at the boundary between the media and adventitia. A peak circumferential stress occurred in the media at the boundary between the media and adventitia under a physiological condition, and an almost flat distribution was obtained in the adventitia. This pattern does not change under a hypertensive condition. These results suggest that a remodeling with hypertension occurs in the media. [DOI: 10.1115/1.4007863]

Keywords: left anterior descending coronary artery, bilayer model, residual strain and stress

1 Introduction

Cardiovascular tissues are subject to residual stress, i.e., there is nonzero stress in a body when all external forces are removed [1–6]. For arteries, a stress concentration obtained by an analysis based on the finite deformation theory, a nonlinear constitutive law, and the assumption of zero initial stress [7–9] is very severe at the intraluminal surface of a vessel wall under physiological loads. Chuong and Fung [10] first demonstrated that residual stress (strain) can considerably alter stress distribution in arterial walls under physiological conditions, i.e., a severe stress concentration is compensated with the circumferential residual stress, which is compressive on the inner side and tensile on the outer side. Takamizawa and Hayashi [7,11] proposed a uniform-strain hypothesis in which circumferential strain is uniformly distributed throughout the wall thickness under a physiological condition. However, this assumption has not been generally supported by experiments on arteries, i.e., it has been demonstrated that the opening angle, which is defined as the angle subtended between two lines originating from the midpoint to the tips of the inner surface of a radial section of the vessel ring. This strongly depends on the site of the aorta [3], and in some arteries the opening angles are greater than 180 deg [12,13], although the uniform-strain hypothesis gives an opening angle less than 180 deg [11]. These results indicate that stress distribution under physiological loads is not so uniform that the uniform-strain hypothesis applies [10,14]. Each one of the approaches mentioned above assumes a monolayer homogeneous wall. However, the arterial wall is a multilayer structure that consists of the adventitia, media, and intima [15]. When the wall stress generated by pressurization and axial extension is considered, the intima is negligible because it is significantly thinner than the other two layers [15], although the intima of coronary arteries of an aged human is of comparable thickness to the other two layers [16]. Although residual stress was not considered in this study, the mechanical properties of a bilayer model of bovine carotid arteries were analyzed by von Maltzhan et al. [17] who used an exponential strain energy function proposed by Fung et al. [18]. For porcine coronary arteries, the three-dimensional mechanical properties were investigated considering residual stress by Wang et al. [19], i.e., they determined the material constants of the exponential strain energy density function proposed by Chuong and Fung [8] for separated adventitia and media. In porcine coronary arteries, the opening angle of the adventitial rings was less than 180 deg, whereas the opening angle of the medial rings was greater than 180 deg. These results give a large difference in stress and strain distributions between the adventitial and medial layers of a right coronary artery [20].

In this study, we propose a method for analyzing strain and stress distribution in soft tissues with residual stress [21,22] and apply it to a porcine left anterior descending coronary artery (LAD). In this analysis, an elastic bilayer model is used for the artery considering that each layer has a different opening angle and material constants. First, strain and stress distribution under a no-load condition were calculated. Second, the outer radius versus intraluminal pressure and the axial force versus intraluminal pressure relations were computed at three different axial stretch ratios. Thereafter, the strain and stress distributions under physiological loads were computed.

2 Methods

2.1 Kinematics. Let $\mathscr{B}$ be a set of material points, and a configuration χ a mapping from $\mathscr{B}$ into three-dimensional Euclidean space, i.e., $\chi : \mathscr{B} \rightarrow \mathbf{E}^3$. A curvilinear coordinate system $[O; x^1, x^2, x^3; g_{kl}(k, l = 1, 2, 3)]$ is introduced into the Euclidean space $\mathbf{E}^3$. Here, O designates the origin of the coordinate system, x^k $(k = 1, 2, 3)$ are coordinates of a material point p, i.e., $\mathbf{x} = (x^1, x^2, x^3) = \chi(p)$ and g_{kl} are components of a metric tensor. In general, there may not be a configuration in which the stress is zero all over a body, even if all external forces are removed from

[1]Corresponding author.

Manuscript received October 26, 2011; final manuscript received October 10, 2012; accepted manuscript posted October 22, 2012; published online May 16, 2013. Assoc. Editor: Krishna Garikipati.

the body. However, a local stress-free configuration can be defined. A local configuration for a material point, p, is defined as $\kappa_p : U_p \rightarrow \mathbf{E}^3$, where U_p is a set of material points such that $p \in U_p \subset \mathscr{B}$. A local stress-free configuration, κ_p, is defined as a local configuration that stress is equal to zero, at least, at $\kappa_p(p)$. We can define a set of local stress-free configurations $\mathscr{F} = \{\kappa_p : p \in \mathscr{B}\}$ for the material body $\mathscr{B}$. It is evident that $\mathscr{F}$ is not unique because any rigid body motion, Ω_p, following κ_p gives another local stress-free configuration, i.e., we can take $\mathscr{F}' = \{\kappa_p' : \kappa_p' = \Omega_p \circ \kappa_p \wedge p \in \mathscr{B}\}$. Here, $\Omega_p \circ \kappa_p$ is a composition of two mappings $\Omega_p : \mathbf{E}^3 \rightarrow \mathbf{E}^3$ and κ_p.

The deformation gradient of the current configuration with regard to a local configuration is defined as follows:

$$\mathbf{F} = \frac{\partial \mathbf{x}}{\partial \mathbf{X}} = \left(\frac{\partial x^k}{\partial X^K}\right) \tag{1}$$

where $\mathbf{x} = \chi(\kappa_p^{-1}(\mathbf{X}))$ and $\mathbf{X} = \kappa_p(q)$ for $q \in U_p$. It should be noted that the definition is valid in a general case at $q = p$ because we only know that the stress at the point $\mathbf{X} = \kappa_p(p)$ is certainly zero. Therefore, we take another local stress-free configuration for another material point, p'. However, if the stress is zero for every material point $q \in U_p$, the definition of the above deformation gradient is valid for every $\mathbf{X} \in \kappa_p(U_p)$. If there is a stress-free configuration $\kappa : \mathscr{B} \rightarrow \mathbf{E}^3$, we can take $\kappa_p = \kappa$ for every $p \in \mathscr{B}$. This is a conventional case of a stress analysis for a solid body.

The infinitesimal volume dV at $\mathbf{X} = \kappa_p(p)$ in the local stress-free configuration is expressed as follows:

$$dV = \sqrt{G} dX^1 dX^2 dX^3 \tag{2}$$

where $G = \det(G_{KL}) = \det(g_{KL}(\mathbf{X}))$. The corresponding volume dv in the current configuration is

$$dv = J\sqrt{g} dX^1 dX^2 dX^3 \tag{3}$$

where $g = \det(g_{kl})$ and $J = \det \mathbf{F}$, and where ρ_o and ρ denote a material density at $\mathbf{X} = \kappa_p(p)$ in the local stress-free configuration and one at $\mathbf{x} = \chi(p)$ in the current configuration, respectively, the mass conservation law is expressed as follows:

$$\rho_o \sqrt{G} = \rho J \sqrt{g} \tag{4}$$

If the material is incompressible, the volume is conserved. From Eqs. (2) and (3), the following equation is satisfied:

$$\sqrt{G} = J\sqrt{g} \tag{5}$$

The components of Green strain in the current configuration χ are expressed as follows:

$$E_{KL} = \frac{1}{2}\left(\frac{\partial x^k}{\partial X^K}\frac{\partial x^l}{\partial X^L} g_{kl} - G_{KL}\right) \tag{6}$$

It is evident that $E_{KL} = E_{LK}$.

When a straight tube is the subject, we adopt a cylindrical coordinate system for convenience, $x^1 = \theta, x^2 = z, x^3 = r$. The metric tensor of the cylindrical coordinate system is given as follows: $g_{11} = g_{\theta\theta} = r^2$, $g_{22} = g_{zz} = 1$, $g_{33} = g_{rr} = 1$, $g_{12} = g_{\theta z} = 0$, $g_{13} = g_{\theta r} = 0$, $g_{21} = g_{z\theta} = 0$, $g_{23} = g_{zr} = 0$, $g_{31} = g_{r\theta} = 0$, $g_{32} = g_{rz} = 0$. For stress-free bodies, we adopt $X^1 = \Theta$, $X^2 = Z$, $X^3 = R$, In the same manner as the above equations, $G_{11} = G_{\Theta\Theta} = R^2$, $G_{22} = G_{ZZ} = 1$, $G_{33} = G_{RR} = 1$, $G_{12} = G_{\Theta Z} = 0$, $G_{13} = G_{\Theta R} = 0$, $G_{21} = G_{Z\Theta} = 0$, $G_{23} = G_{ZR} = 0$, $G_{31} = G_{R\Theta} = 0$, $G_{32} = G_{RZ} = 0$.

The stress-free states for the adventitia and media of porcine LAD are schematically shown in Fig. 1. In this study, the loading of the intraluminal pressure and the uniform axial stretch did not produce any shear strain in the cylindrical coordinate system because a cylindrical orthotropy was assumed [23]. The values of various dimensions in stress-free states are presented in Table 1. The opening angles of the stress-free states of the adventitia and media sectors are from Lu et al. [24]. The radii of the sectors of the adventitia and media were estimated from the data by Wang et al. [25], assuming that the adventitial and medial thicknesses are equal because the separated adventitia and media thicknesses were not provided.

Let the artery be loaded with an intraluminal pressure P_i and an axial stretch ratio λ_z. The radius of the intraluminal surface becomes r_i, the radius of the boundary between adventitia and media r_m, and the outer radius r_o. The radius of the intraluminal surface in the stress-free state is R_{Mi}, and the radius of the media at the boundary between the media and adventitia R_{Mo}. Thus, the deformation of the media is expressed as follows:

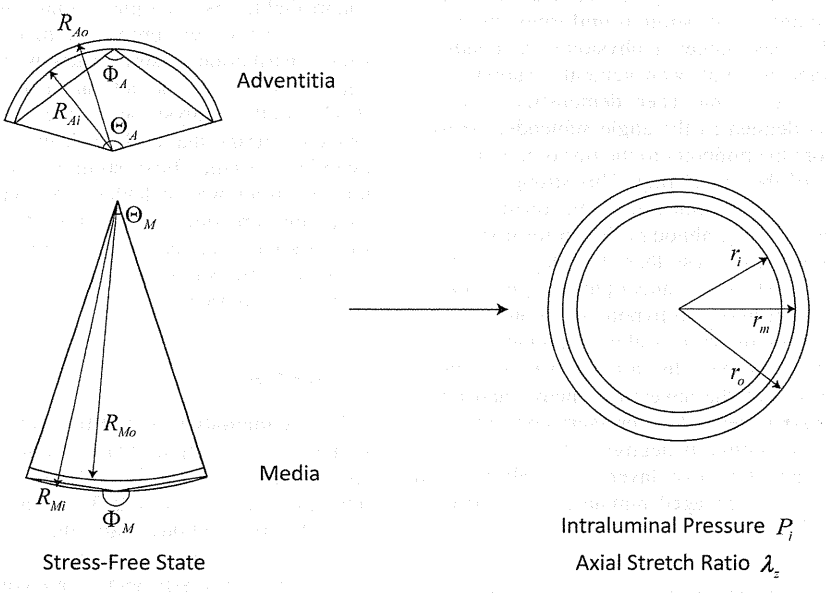

Fig. 1 Schematic drawing of stress-free state of adventitia and media, and loaded state of intact vessel

Table 1 Stress-free sectors of media and adventitia of LAD

Media	
$\Phi_M = 198$ deg	$\Theta_M = 36$ deg
$R_{Mi} = 13.620$ mm	$R_{Mo} = 13.306$ mm
Adventitia	
$\Phi_A = 108$ deg	$\Theta_A = 144$ deg
$R_{Ai} = 3.199$ mm	$R_{Ao} = 3.513$ mm

$$\begin{aligned} &\theta = \frac{2\pi}{\Theta_M}(\Theta_M - \Theta) \quad (0 \le \Theta \le \Theta_M, 0 \le \theta \le 2\pi) \\ &z = \lambda_z Z \\ &r = r(R) \quad (R_{Mo} \le R \le R_{Mi}, r_i \le r \le r_m) \end{aligned} \tag{7}$$

where angles are expressed in radians and $\Theta_M = 2(\Phi_M - \pi)$ for the opening angle Φ_M is larger than π(rad). Because the incompressibility of the media is expressed by Eq. (5), the following relation is satisfied:

$$R = \sqrt{R_{Mo}^2 + \frac{2\pi\lambda_z(r_m^2 - r^2)}{\Theta_M}} \tag{8}$$

The Green strain component $E_{11} = E_{\Theta\Theta}$ is expressed as follows:

$$E_{\Theta\Theta} = \frac{1}{2}\left\{\left(\frac{2\pi r}{\Theta_M}\right)^2 - R^2\right\} \tag{9}$$

where the subscript for the Green strain components follows the manner of subscript for the metric tensor components. The physical component of $E_{\Theta\Theta}$ is defined by the following equation:

$$\overline{E}_{\Theta\Theta} = \frac{E_{\Theta\Theta}}{\sqrt{G_{\Theta\Theta}}\sqrt{G_{\Theta\Theta}}} = \frac{1}{2}\left\{\left(\frac{2\pi r}{\Theta_M R}\right)^2 - 1\right\} \tag{10}$$

Here, $\overline{E}_{\Theta\Theta}$ increases from the intraluminal surface to the boundary between the media and adventitia as $R(r)$ monotonically decreases from r_i to r_m as shown in Eq. (8). In the same manner, the other two physical components $\overline{E}_{ZZ} = E_{ZZ}$ and $\overline{E}_{RR} = E_{RR}$ are represented as follows:

$$\overline{E}_{ZZ} = \frac{1}{2}(\lambda_z^2 - 1), \quad \overline{E}_{RR} = \frac{1}{2}\left\{\left(\frac{\partial r}{\partial R}\right)^2 - 1\right\} \tag{11}$$

The shear components are zero from Eq. (7). Hence, we represented $E_\theta = \overline{E}_{\Theta\Theta}, E_z = \overline{E}_{ZZ}, E_r = \overline{E}_{RR}$.

In the adventitia the deformation is expressed as follows:

$$\begin{aligned} &\theta = \frac{2\pi}{\Theta_A}\Theta \quad (0 \le \Theta \le \Theta_A, 0 \le \theta \le 2\pi) \\ &z = \lambda_z Z \\ &r = r(R) \quad (R_{Ai} \le R \le R_{Ao}, r_m \le r \le r_o) \end{aligned} \tag{12}$$

where $\Theta_A = 2(\pi - \Phi_A)$ for the opening angle Φ_A is smaller than π(rad). Because the incompressibility is expressed by Eq. (5), the relation between R and r in the adventitia is represented as follows:

$$R = \sqrt{R_{Ao}^2 - \frac{2\pi\lambda_z(r_o^2 - r^2)}{\Theta_A}} \tag{13}$$

The Green strain components and their physical components are represented in the same manner for the media.

2.2 Strain Energy Density Function. W represents a strain energy density, i.e., the elastic energy stored per unit volume of a stress-free body. Although an artery is a viscoelastic material, a strain energy density function is used for convenience. The strain energy function describes the repeatable behaviors of cardiovascular tissues following several cyclic loading and unloading events. In this study, the exponential strain energy density function [8] was used

$$W = \frac{C}{2}(\exp Q - 1) \quad Q = b^{KLMN}E_{KL}E_{MN} \tag{14}$$

where b^{KLMN} represent the contravariant components of a tensor. It should be noted that the physical components are the material constants and that they are different between the media and adventitia. As Q is a quadratic form of the strain components, the following symmetry of the coefficients may be induced without loss of generality:

$$b^{KLMN} = b^{MNKL} = b^{LKMN} = b^{LKNM} \tag{15}$$

For the cylindrical orthotropic material, the coefficients $b^{\Theta\Theta\Theta\Theta}$, b^{ZZZZ}, b^{RRRR}, $b^{\Theta\Theta ZZ}$, b^{ZZRR}, $b^{RR\Theta\Theta}$, $b^{\Theta Z\Theta Z}$, b^{ZRZR}, $b^{R\Theta R\Theta}$ and components, which are allowed by the symmetry (Eq. (15)) with superscripts to match the above ones, may have nonzero values. The other components must be zero because of the cylindrical orthotropy validated by the experiments [23]. The physical components of the coefficients are given as follows:

$$\begin{aligned} &\overline{b}^{KLMN} = \sqrt{G_{KK}}\sqrt{G_{LL}}\sqrt{G_{MM}}\sqrt{G_{NN}}b^{KLMN} \\ &(K, L, M, N \text{ not summed}) \end{aligned} \tag{16}$$

where the above physical components are the material constants and the difference between the media and adventitia.

The stress-strain relation is expressed as follows:

$$t^{kl} = \frac{1}{J}\sqrt{\frac{G}{g}}\frac{\partial x^k}{\partial X^K}\frac{\partial x^l}{\partial X^L}\frac{\partial W}{\partial E_{KL}} \tag{17}$$

where t^{kl} are contravariant components of the Cauchy stress tensor. If the material is incompressible, Eq. (5) must be satisfied. This constraint induces the Lagrange multiplier H into Eq. (17),

$$\begin{aligned} t^{kl} &= -Hg^{kl} + \frac{\partial x^k}{\partial X^K}\frac{\partial x^l}{\partial X^L}\frac{\partial W}{\partial E_{KL}} \\ &= -Hg^{kl} + C\exp Q\frac{\partial x^k}{\partial X^K}\frac{\partial x^l}{\partial X^L}b^{KLMN}E_{MN} \end{aligned} \tag{18}$$

where g^{kl} represents the (k, l) component of the reciprocal metric tensor. Because only the principal components of the Green strain may not be zero, Q is represented as follows:

$$\begin{aligned} Q &= b^{\Theta\Theta\Theta\Theta}E_{\Theta\Theta}^2 + b^{ZZZZ}E_{ZZ}^2 + b^{RRRR}E_{RR}^2 \\ &\quad + 2(b^{\Theta\Theta ZZ}E_{\Theta\Theta}E_{ZZ} + b^{ZZRR}E_{ZZ}E_{RR} + b^{RR\Theta\Theta}E_{RR}E_{\Theta\Theta}) \\ &= \overline{b}^{\Theta\Theta\Theta\Theta}\overline{E}_{\Theta\Theta}^2 + \overline{b}^{ZZZZ}\overline{E}_{ZZ}^2 + \overline{b}^{RRRR}\overline{E}_{RR}^2 \\ &\quad + 2(\overline{b}^{\Theta\Theta ZZ}\overline{E}_{\Theta\Theta}\overline{E}_{ZZ} + \overline{b}^{ZZRR}\overline{E}_{ZZ}\overline{E}_{RR} + \overline{b}^{RR\Theta\Theta}\overline{E}_{RR}\overline{E}_{\Theta\Theta}) \end{aligned} \tag{19}$$

The physical components of the Cauchy stress tensor are defined as follows:

$$\overline{t}^{kl} = \sqrt{g_{kk}}\sqrt{g_{ll}}t^{kl} \quad (k, l \text{ not summed}) \tag{20}$$

Considering the above relations, the physical components of the Cauchy stress are expressed in the physical components of the Green strain as follows:

Table 2 Material constants of strain energy density function for media and adventitia of LAD

	C	$\bar{b}^{\Theta\Theta\Theta\Theta}$	$\bar{b}^{ZZZZ}$	$\bar{b}^{RRRR}$	$\bar{b}^{\Theta\Theta ZZ}$	$\bar{b}^{ZZRR}$	$\bar{b}^{RR\Theta\Theta}$
Media	5.11 kPa	2.47	3.09	0.95	0.45	0.06	0.10
Adventitia	9.05 kPa	0.62	2.27	1.67	0.34	0.11	0.07

$$\bar{t}^{\theta\theta} = -H + C\exp Q\left(\frac{r\,\partial\theta}{R\,\partial\Theta}\right)^2\left(\bar{b}^{\Theta\Theta\Theta\Theta}\bar{E}_{\Theta\Theta} + \bar{b}^{\Theta\Theta ZZ}\bar{E}_{ZZ} + \bar{b}^{\Theta\Theta RR}\bar{E}_{RR}\right)$$
$$\bar{t}^{zz} = -H + C\exp Q\left(\frac{\partial z}{\partial Z}\right)^2\left(\bar{b}^{ZZ\Theta\Theta}\bar{E}_{\Theta\Theta} + \bar{b}^{ZZZZ}\bar{E}_{ZZ} + \bar{b}^{ZZRR}\bar{E}_{RR}\right)$$
$$\bar{t}^{rr} = -H + C\exp Q\left(\frac{\partial r}{\partial R}\right)^2\left(\bar{b}^{RR\Theta\Theta}\bar{E}_{\Theta\Theta} + \bar{b}^{RRZZ}\bar{E}_{ZZ} + \bar{b}^{RRRR}\bar{E}_{RR}\right) \tag{21}$$

and $\bar{t}^{kl} = 0$ $(k \neq l)$ because there are no shear strain components. Hence, we represent $\sigma_k = \bar{t}^{kk}$. The seven material constants for the media and the adventitia are from the study by Wang et al. [19], as shown in Table 2.

2.3 Equilibrium Equation of Cauchy Stress. The equations for the Cauchy stress equilibrium are given as follows [26]:

$$t^{kl}_{;k} = \frac{\partial t^{kl}}{\partial x^k} + \Gamma^l_{km}t^{km} + \Gamma^m_{km}t^{kl} = 0 \tag{22}$$

where $;k$ denotes the covariant differentiation with coordinate x^k, and Γ^l_{km} are the Christoffel symbols of the second kind. In a cylindrical vessel wall subject to an intraluminal pressure and a constant longitudinal stretch, only the following equilibrium equation for the physical components of the Cauchy stress is nontrivial:

$$\frac{\partial\sigma_r}{\partial r} + \frac{\sigma_r - \sigma_\theta}{r} = 0 \tag{23}$$

The boundary conditions are represented as follows:

$$\sigma_r(r_i) = -P_i, \quad \sigma_r(r_o) = -P_o = 0 \tag{24}$$

where P_i is the intraluminal pressure of the vessel and P_o is the pressure of the outer surface. The integral form of Eq. (23) with the boundary condition of Eq. (24) is expressed as follows:

$$\sigma_r(r) = -P_i + \int_{r_i}^{r}\frac{\sigma_\theta(\xi) - \sigma_r(\xi)}{\xi}d\xi \tag{25}$$

Here, it should be noted that the integrand does not include the Lagrange multiplier H. The integral in Eq. (25) was computed using the Simpson's trapezoidal rule for each layer. The outer boundary condition determines the intraluminal pressure P_i,

$$P_i = \int_{r_i}^{r_o}\frac{\sigma_\theta(r) - \sigma_r(r)}{r}dr \tag{26}$$

The Lagrange multiplier H as a function of r can be calculated by the following equation:

$$H(r) = C\exp Q\left(\frac{\partial r}{\partial R}\right)^2\left(\bar{b}^{RR\Theta\Theta}\bar{E}_{\Theta\Theta} + \bar{b}^{RRZZ}\bar{E}_{ZZ} + \bar{b}^{RRRR}\bar{E}_{RR}\right) - \sigma_r(r) \tag{27}$$

The radial stress is continuous at the boundary between media and adventitia, although H may be discontinuous at the boundary. The other principal components σ_θ and σ_z can be calculated from Eq. (21). The axial stretch force F_z at the intraluminal pressure P_i and the stretch ratio λ_z is calculated by the following equation:

$$F_z = -\pi r_i^2 P_i + 2\pi\int_{r_i}^{r_o}\sigma_z r dr = 2\pi\int_{r_i}^{r_o}\left\{\sigma_z - \frac{1}{2}(\sigma_\theta + \sigma_r)\right\}r dr \tag{28}$$

where the integral was computed by the numerical method using Eq. (21). If the stress-free states and the constitutive law are provided, the intraluminal pressure and the axial force are calculated as functions of the axial stretch ratio λ_z and another parameter, for example, the outer radius r_o. Therefore, the intraluminal pressure and axial force were numerically computed for a given radius and axial stretch ratio, $P_i = P_i(\lambda_z, r_o)$ and $F_z = F_z(\lambda_z, r_o)$. The residual stress and strain can be determined by the conditions of $P_i = 0$ and $F_z = 0$. The radius and axial stretch ratio satisfying these conditions were computed by an iteration method.

3 Results

Figure 2 shows the residual strain and stress in the media and adventitia as computed using the data in Tables 1 and 2. The residual circumferential strain is compressive in the inner region and tensile in the outer region. The discontinuity occurs at the boundary between the media and adventitia. However, the strain begins to be tensile in the media. The axial strain is negative although its magnitude is very small as shown in Fig. 2(*a*). The residual axial stress is compressive in the inner region and tensile in the outer region. The magnitude of the residual stress is very small compared with the stress under physiological conditions, although the magnitude of the residual circumferential and radial strains is not so small compared with the physiological one.

Computations were performed to determine the intraluminal pressure and the axial force for a given outer radius and axial stretch ratio of a vessel. Figure 3 shows the outer radius versus

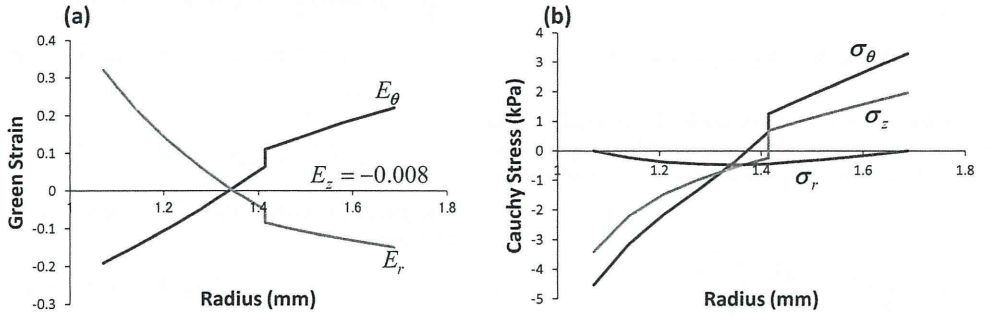

Fig. 2 Distributions of strain (*a*) and stress (*b*) in the vessel wall under unloaded condition. The boundary between media and adventitia is a position where the discontinuity of distributions of strain and stress appears.